Above-threshold-dissociation dynamics of H_2^+ with short intense laser pulses

G. Jolicard
Laboratoire de Physique Moléculaire, Faculté des Sciences de Besançon, La Bouloie, route de Gray, 25030 Besançon CEDEX, France

O. Atabek
Laboratoire de Photophysique Moléculaire du CNRS, Bâtiment 213, Université de Paris–Sud, 91405 Orsay CEDEX, France
(Received 31 January 1992)

A rigorous time-dependent wave-operator method within the Bloch formalism is presented and applied to the calculation of the photodissociation rate of H_2^+ in intense pulsed laser fields. The wave packet is simultaneously propagated on the radiatively coupled ground and electronically excited potential-energy surfaces of the ion, combining a Lanczos reduction technique at low orders and recursive time-dependent Bloch operators. Dissociation rates are extracted from an asymptotic-flow analysis in the momentum space. The energy distributions of the protons, resulting from multiphoton absorption above the dissociation threshold, consist of a sequence of peaks spaced by half of the photon energy. The distribution of higher-energy peaks decreases with increasing intensity, due to stimulated emission from dissociating fragments. Time-resolved dynamics reached by ultrashort intense pulses ($\simeq$20-fs duration and peak intensity varying in the range from 3.5×10^{12} to 3.5×10^{14} W/cm^2) leads to a thorough interpretation of photon-exchange mechanisms between the field and the ion during the excitation and fragmentation steps.

PACS number(s): 33.80.Gj, 33.80.Eh

I. INTRODUCTION

With the advent of intense lasers, an increased amount of attention has recently been directed to the study of photodissociation dynamics both from experimental and theoretical viewpoints. It is now a well-known fact that atoms irradiated by intense laser light exhibit some singular behaviors such as above-threshold ionization (ATI) by absorbing more photons than the minimum needed to ionize [1]. Similar nonlinear phenomena have also been observed in molecules [2–4] with an experimental signature being the appearance of successive peaks separated by one quantum of photon energy in the kinetic-energy distribution of the ejected photoelectrons. Their additional interatomic degrees of freedom make the study of molecules even more challenging. Very complicated behaviors may be observed even with simple diatomic molecules, including multiphoton above-threshold dissociation (ATD), which can be evidenced by the observation of peaks in the kinetic-energy spectrum of the atomic photofragments [4] spaced as in the ionization case by one quantum of photon energy.

Many photons are absorbed by free-state–free-state transitions once the molecule is already in the dissociation continuum. During the process of falling apart, most of the absorbed energy is returned to the electromagnetic field via stimulated emissions, which cause a slowing down of the fragments. The possibility of this new phenomenon has recently been examined by referring to time-dependent scattering calculations [5] and experimentally confirmed by studying multiphoton dissociation of H_2^+ in laser fields with strengths comparable to the internuclear binding energies (i.e., $\simeq$50 TW/cm^2) [4]:

$$H_2^+(1s\sigma_g,v)+n\hbar\omega\rightarrow H_2^+(2p\sigma_u)\rightarrow H^+ + H(1s)+\varepsilon(n)\ .$$

The ion-dissociation spectra have multiple peaks caused by multiphoton transitions during dissociation of H_2^+. Theory predicts a similar behavior by finding that multiphoton absorption can easily lead [even in modest fields $\simeq10^7$ W/cm^2) to dissociation pathways involving more photons than the minimum number required (ATD)].

Experimental data suggest that the molecule might deform due to its multiphoton coupling with the laser field, leading to "bond softening," which results in dissociation at laser intensities over 50 TW/cm^2. Some theoretical works seem to confirm such a possibility [5–13].

Even more surprising is the distribution of higher-energy peaks in the photofragment spectrum, which decreases with increasing intensity due to stimulated free-state–free-state emission of the dissociating fragments [5,12,13]. Apart from above-threshold dissociation and bond softening, a vibrational trapping mechanism leading to an important decrease in the dissociation rate at some energies has also been predicted [14] and very recently calculated [15].

A proper theoretical description of such molecular processes induced by intense fields, where Rabi frequencies ($\omega_R=\mu E/\hbar$, with μ the transition moment, and E the electric-field amplitude) are comparable with vibrational spacings, should be nonperturbative to take into account highly nonresonant transitions that compete with resonant ones. The dressed-molecule concept [16] is one possible approach dealing with molecular electronic potential-energy surfaces adiabatically modified by the laser field. A molecule-field coupled-channel formalism is used to treat simultaneously radiative and nonradiative interactions. Laser-induced resonances, which obviously are beyond the scope of perturbative techniques, can be predicted. Their interpretation is attempted in terms of Feshbach resonances in a diabatic picture involving all

photon-number states introduced through the Floquet analysis, or in terms of shape resonances in an adiabatic representation [6,17,18]. Time-independent quantum close-coupled formulations that have so far been developed either refer to a full-collision [5,12,13,19] or a half-collision process [6,17,18]. Artificial channels [12,13] or complex rotation of the nuclear coordinate [6,17,18] are some variants of these methods, yielding not only the total broadening, resultant dissociation rate, and associated ac Stark shift of the initial bound state, but also branching ratios into specific open channels corresponding to varying amounts of absorbed photons. Time-dependent approaches have only recently been addressed and are in the developing state. In particular, wave-packet calculations of multiphoton dissociation by infrared lasers have already demonstrated the possibility of ADT for a single electronic state [7].

More recently, wave-packet propagations by repeated application of short-time propagators in the split-operator form [8] have been performed on intense-field photodissociation of H_2^+ [9,10]. These calculations aim to compare time-dependent and -independent results, and are thus basically referring to cw lasers or continuous lasers that are switched following a smooth adiabatic pathway.

This paper presents a time-dependent wave-operator theory within Bloch formalism to study the multiphoton dissociation of H_2^+, stressing the sensitivity of the resulting kinetic-energy distributions with respect to the pulse shape and intensity of the electromagnetic field. The propagation technique, which is well adapted to the fast changes of the field, appears to be very effective in the present context. The time-dependent description, apart from giving a physically appealing dynamical picture, allows the possibility, through the use of ultrashort laser pulses, of probing the photodissociation process during and after the excitation, while the products fall apart. An additional advantage, at least in the case of H_2^+, is that difficulties related to the use of the length or velocity gauges [5] can simply be relaxed by the use of pulsed lasers. Using the dipole approximation, the molecule-field coupling in the length (electric field) gauge $\mu\mathbf{E}$ asymptotically diverges for the $1s\sigma_g \rightarrow 2p\sigma_u$ transition in H_2^+ [20], which causes the violation of the requirement that in a proper scattering theory the channel states must be uncoupled at infinite separation. This is why in time-independent approaches one has either to consider the velocity (radiative field) gauge $\mathbf{A}\cdot\mathbf{p}$ [5] or to use some mathematical artifacts such as the complex rotation of the nuclear coordinate [6]. Gauge invariance can be assured only if a complete set of electronic states is considered. The results are actually highly sensitive to the choice of gauge when expanding the wave function on solely two electronic states [11]. With pulsed lasers, clearly no asymptotic divergence can be obtained due to the finite duration of the radiative coupling. Contrary to previous time-dependent calculations [9,10], where the purpose is to demonstrate the agreement with time-dependent results using cw lasers, we proceed with the length gauge that is more appropriate.

Section II presents briefly the essential features of the time-dependent propagation technique by emphasizing the following steps: (i) the so-called discrete-variable representation (DVR) of the Hamiltonian; (ii) the wave-packet propagation simultaneously on the two radiatively coupled potential-energy surfaces ($1s\sigma_g$ and $2p\sigma_u$) using Lanczos technique at low orders to initiate the recursive time-dependent Bloch-operators method; (iii) the analysis of quantum fluxes in momentum space. Section III is a general discussion of the time-resolved dynamics, as a function of the field intensity, starting from early excitation events, where the laser pulse monitors the preparation step with an excited-state population oscillating in phase with the field, to final dissociation probabilities after absorption of a net amount of one, two, or three photons. The way in which the radiative field and the molecule adiabatically exchange photons is examined. As in previous works, it seems that the initial decay of the resonance is catalyzed by energy borrowed from the radiation field in terms of absorbed photons, which are subsequently returned to the field via stimulated emissions. Considering the adiabatic nature of these exchanges, it appears that higher-energy peaks corresponding to fast protons are less likely with increasing field intensity.

II. THEORY

The aim of this section is to give an overall comprehensive view of the theory and deals with the time evolution of a wave function $\Psi(R,t)$ under the action of a time-dependent Hamiltonian $H(t)$. The Schrödinger equation governing this evolution is

$$i\hbar\frac{d}{dt}\Psi(R,t)=\mathbf{H}(t)\Psi(R,t)\ , \tag{1}$$

where R designates the dissociative nuclear coordinate. The Hamiltonian itself, in the Born-Oppenheimer approximation, involves two electronic states (i.e., the ground g and excited u states) that are radiatively coupled:

$$\mathbf{H}(t)=\begin{bmatrix} -\frac{1}{2}\frac{d^2}{dR^2}+V_g(R) & -\mu_{gu}(R)E(t) \\ -\mu_{ug}(R)E(t) & -\frac{1}{2}\frac{d^2}{dR^2}+V_u(R) \end{bmatrix}. \tag{2}$$

$V_g(R)$ and $V_u(R)$ are the corresponding potential energies and $\mu_{gu}(R)$ the electronic transition dipole moment. In the absence of any field, the ion is supposed to be at the $v=0$ vibrational level of its ground state g. The electromagnetic-field amplitude $E(t)$ is given as the product of a time-dependent shape function $\varepsilon(t)$ by a real cosine form, with peak frequency ω:

$$E(t)=\varepsilon(t)\cos\omega t\ . \tag{3}$$

A. Discrete-variable representation of the Hamiltonian

The implementation of the so-called discrete-variable representation requires (i) a basis set $\{\psi_n(R),\ n=1-N\}$ in which to expand the wave function of a system, and (ii)

a Gauss quadrature rule with a set of quadrature points $\{R_n,\ n=1-N\}$ and weights $\{w_n,\ n=1-N\}$ to compute matrix elements in this basis [21]. When these conditions are fulfilled, there exists an isomorphism between the finite basis representation (FBR) in terms of $\{\psi_n\}$ and a basis of coordinate eigenfunctions $\{u_j\}$ satisfying the Kronecker-δ property [22]:

$$u_j(R_k)=\delta_{jk} \ . \tag{4}$$

We follow here the derivation given by Muckerman [23], taking as the original basis $\{\psi_n\}$ the properly normalized particle-in-a-box eigenfunctions:

$$\psi_n(R)=\left[\frac{2}{R_{\max}-R_{\min}}\right]^{1/2}\sin\left[n\pi\frac{R-R_{\min}}{R_{\max}-R_{\min}}\right] \quad (n=1-N) \ . \tag{5}$$

This choice together with equally spaced quadrature points on the radial axis, given by

$$R_n=R_{\min}+n(R_{\max}-R_{\min})/(N+1) \quad (n=1-N) \tag{6}$$

and adjusted equal weights

$$w_n=(R_{\max}-R_{\min})/(N+1) \quad (n=1-N) \tag{7}$$

lead through the above-mentioned isomorphism, which is nothing but a discrete real sine Fourier transform, to the DVR basis set

$$u_n(R)=w_n\sum_{j=1}^{N}\psi_j(R)\psi_j^*(R_n) \quad (n=1-N) \ . \tag{8}$$

Equation (8) is the central result of the DVR approach and defines an analytically computable basis satisfying the Kronecker property [Eq. (4)].

The time-dependent wave function $\Psi(R,t)$ is expanded in the orthogonal (but not normalized) DVR basis:

$$\Psi(R,t)=\sum_{n=1}^{N}\Psi(R_n,t)u_n(R) \ . \tag{9}$$

We note that in a time-independent calculation of energy eigenvalues and eigenfunctions the use of the orthonormal basis $\{w_n^{-1/2}u_n(R)\}$ would be more convenient. Equation (9) presents in time-dependent problems the advantage that the expansion coefficients are the values of the wave function at the grid points. The application of a coordinate operator $V(R)$ followed by an evaluation at a grid point is straightforward and yields a diagonal representation,

$$V(R)\Psi(R,t)\Big|_{R=R_k}=\sum_{n=1}^{N}\Psi(R_n,t)V(R_k)u_n(R_k) = V(R_k)\Psi(R_k) \ , \tag{10}$$

when use is made of Eq. (4).

As for the kinetic-energy operator, one has

$$\frac{d^2}{dR^2}\Psi(R,t)\Big|_{R=R_k}=\sum_{n=1}^{N}\Psi(R_n,t)\frac{d^2}{dR^2}u_n(R)\Big|_{R=R_k} \ , \tag{11}$$

where

$$\frac{d^2}{dR^2}u_n(R)\Big|_{R_k}=\frac{1}{N+1}\sum_{j=1}^{N}\frac{2j^2\pi^2}{(R_{\max}-R_{\min})^2}\times\sin\left[\frac{\pi kj}{N+1}\right]\sin\left[\frac{\pi nj}{N+1}\right] \tag{12}$$

is clearly nondiagonal.

The representation of the Hamiltonian Eq. (2) in the DVR basis can be obtained by calculating the matrix elements of H_{ij} using Gauss quadratures, i.e.,

$$H_{ij}=\int h_{ij}(R)dR=\sum_{k=1}^{N}w_k h_{ij}(R_k) \quad (i,j=1-N) \ , \tag{13}$$

where

$$h_{ij}=u_i^*(R)\left[-\frac{1}{2}\frac{d^2}{dR^2}+V_{g,d}(R)\right]u_j(R) \tag{14a}$$

on the diagonal block of Eq. (2) or

$$h_{ij}=u_i^*(R)[-\mu_{gd}(R)E(t)]u_j(R) \tag{14b}$$

on the off-diagonal block of Eq. (2).

The $(2N\times 2N)$ Hamiltonian matrix that results is very sparse as in all DVR methods. It can simply be calculated analytically (without any inaccuracy) combining Eqs. (10)–(12), and its general form is schematically indicated in Fig. 1. The two $(N\times N)$ diagonal blocks describe the ground- (g) and excited- (u) state Hamiltonians with matrix elements given by

$$H_{ij}^{g(u)}=\left[\frac{R_{\max}-R_{\min}}{N+1}\right]\left[-\frac{1}{2}\frac{d^2u_j}{dR^2}(R)\Big|_{R_i}+V_{g(u)}(R_i)\delta_{ij}\right] \ , \tag{15a}$$

where the values taken by the electronic potential energies (V_g or V_u) at the grid points only contribute as diagonal terms. As for the two $(N\times N)$ off-diagonal blocks describing the radiative coupling, the only nonzero con-

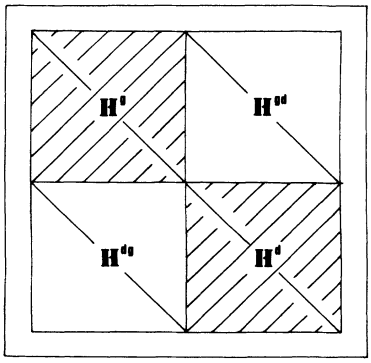

FIG. 1. Schematic representation of the Hamiltonian in the DVR basis.

tributions are

$$H_{ij}^{gd}=-\left[\frac{R_{\max}-R_{\min}}{N+1}\right]\mu_{gu}(R_i)E(t)\delta_{ij} \ . \tag{15b}$$

B. Wave-packet propagation

The time-dependent Bloch wave-operator theory that has been presented elsewhere [24] requires the wave packet to lie at initial time t_0, in a small subspace S_0 of the original Hilbert space where the total Hamiltonian induces the dynamics. It is clear that, when considering long propagation times, the initial wave packet spreads out on a large part of the coordinate space with an increasing number of non-negligible components on the orthogonal basis (taken here as an external sum $u_j \oplus u_n$, $j=1-N$, $n=1-N$ of the vectors spanning the g and u states). This indeed is inconsistent with keeping S_0 small. A way to overcome the difficulty is to introduce an evolutive nonorthogonal basis $\{u'\}$ at each time step t_n by particularizing a vector u_p presenting the largest overlap modulus $|\langle u_p|\Psi(t_n)\rangle|$ with the wave function of the system at time t_n:

$$u_j'(t_n)=\begin{cases} u_j, & j\neq p \qquad (16a)\\ \Psi(t_n), & j=p \ . \qquad (16b)\end{cases}$$

In this new representation, the solution at time $t=t_n$ belongs to a one-dimensional space S_0 spanned by the vector u_p'.

The wave-operator method focuses on the propagation of the solution over the time interval $[t_n,t_{n+1}]$,

$$\Psi(t_{n+1})=U(t_{n+1},t_n;H)u_p' \ , \tag{17}$$

driven by an evolution operator U expressed in terms of the so-called wave operator Ω and the time-dependent effective Hamiltonian H_{eff} [24]:

$$U(t_{n+1},t_n;H)=\Omega(t_{n+1},t_n)P_0U(t_{n+1},t_n;H_{\text{eff}})P_0 \ . \tag{18}$$

$P_0=|u_p'\rangle\langle u_p'|$ and $Q_0=1-P_0$ are the projectors associated with S_0 and its complementary subspace. The wave operator can be partitioned as

$$\Omega(t_{n+1},t_n)=P_0+X(t_{n+1},t_n) \ , \tag{19a}$$

with

$$X(t_{n+1},t_n)=Q_0\Omega(t_{n+1},t_n)P_0 \ , \tag{19b}$$

where the first term P_0 is nothing but the identity over S_0, and the second term X (also called the reduced wave operator) controls transitions towards the complementary subspace S_0^+.

The effective Hamiltonian that drives the internal dynamics inside S_0 is related to the wave operator through

$$H_{\text{eff}}=P_0H\Omega \ , \tag{20}$$

and is associated with the time-evolution operator $U(t,t_n;H_{\text{eff}})$, which (owing to the fact that S_0 is precisely of dimension 1) can simply be written as

$$U(t,t_n;H_{\text{eff}})=\exp\left[-\frac{i}{\hbar}\int_{t_n}^{t}(H_{\text{eff}})_{pp}dt'\right] \ . \tag{21}$$

Finally, the reduced wave operator X satisfies a nonlinear differential equation [24]:

$$i\hbar\frac{\partial}{\partial t}X(t)=Q_0[1-X(t)]H[1+X(t)]P_0 \ , \tag{22}$$

which is the basic relation of the time-dependent wave-operator formulation and is well adapted to an iterative treatment. The method, although nonunitary, can be considered as numerically exact in the sense that the error may be lowered by reducing the time step and/or by resolving Eq. (22) at an arbitrarily high perturbation order. The search for an iterative scheme as a solution for Eq. (22) yields the following set of relations [24]:

$$X=\lim_{M\to\infty}X^{(M)} \ , \tag{23a}$$

$$X^{(M)}(t,t_n)=\sum_{\substack{j\\ j\neq p}}|u_j'\rangle\langle u_p'|\left[-\frac{i}{\hbar}\int_{t_n}^{t}H_{jp}^{(M)}dt'\exp\left[\frac{i}{\hbar}\int_{t_n}^{t}H_{pp}^{(M)}dt'\right]\right] \quad (M>1) \ , \tag{23b}$$

$$H^{(M)}=(1-X^{(M-1)})H(1+X^{(M-1)})-i\hbar\frac{\partial}{\partial t}X^{(M-1)} \ . \tag{23c}$$

This scheme is initiated using the lowest-order reduced operator $X^{(1)}$ obtained from a Lanczos reduced unitary propagator [25] $U_L^{(m)}(t,t_n;H)$ at mth order [26]:

$$X^{(1)}(t,t_n)=\sum_{\substack{j\\ j\neq p}}|u_j'\rangle\langle u_p'|\left[\frac{\langle u_j'|U_L^{(m)}(t,t_n;H)|u_p'\rangle}{\langle u_p'|U_L^{(m)}(t,t_n;H)|u_p'\rangle}\right] \ . \tag{24}$$

The inaccuracies resulting from a pure Lanczos iteration scheme due to the neglect of slow variations of the Hamiltonian $H(t)$ over the time interval $[t_{n+1},t_n]$, are adequately lowered by the use of the Block wave-operator formalism. This appears to be crucial when referring to a fast time dependence (ultrashort or intense pulses, for instance).

C. Flow analysis in the momentum space

As in all wave-packet calculations, the results that are obtained from asymptotic behaviors correspond to an

average energy. If the observables that are referred to are rate coefficients, this may be an advantage. On the contrary, if the energy dependence of the probabilities is looked for, a deconvolution of the wave packet is necessary. Several treatments have been proposed in the literature [24,27,28], some of them based on temporal Fourier analysis of the asymptotic wave packet [28], others on a spatial Fourier analysis of the associated flux [24]. It is this last technique, with an analysis carried out at some large separation where the potential vanishes and before the wave packet is absorbed (by an optical potential, for instance), which is the one retained in this work.

If R_0 denotes an asymptotic point along the radial axis where both interaction and optical potentials have negligible values,

$$R_0 = R_{\min} + (i_0 - 1)\left[\frac{R_{\max} - R_{\min}}{N}\right], \tag{25}$$

the energy dependence of the probabilities can be deduced from an analysis in the momentum space of the outgoing flux calculated at R_0:

$$[{}^{(c)}F^+(t)]_{R_0} = \mathrm{Re}\left[-\frac{i\hbar}{M}{}^{(c)}\Psi^*(R_0,t)\frac{\partial^{(c)}\Psi(R,t)}{\partial R}\bigg|_{R_0}\right], \tag{26}$$

where M is the reduced mass and the index (c) designates the continuum channel associated with either the ground g or the excited u state. A complex exponential discrete Fourier transform applied to the N equally spaced sampling points on the interval $[R_{\min}, R_{\max}]$ of the R axis [Eq. (25)] gives access to a discrete momentum representation of the sampling points, equally spaced in the k space:

$$k_j = 2\pi j/(R_{\max} - R_{\min}), \quad -N/2+1 \le j \le N/2 . \tag{27}$$

When this is combined with the discrete Fourier expansion of $\Psi(R_0,t)$,

$$\Psi(R_0,t) = \sum_{j=-N/2+1}^{N/2} \tilde{\Psi}(k_j,t)\exp[2i\pi(j-1)(i_0-1)/N], \tag{28}$$

Eq. (26) can be rewritten as

$$[{}^{(c)}F^+(t)]_{R_0} = \sum_{j=1}^{N/2}[{}^{(c)}F_{k_j}^+(t)]_{R_0}, \tag{29}$$

with

$$[{}^{(c)}F_{k_j}^+(t)]_{R_0} = \mathrm{Re}\left[{}^{(c)}\Psi^*(R_0,t)\frac{2\pi\hbar(j-1)}{M(R_{\max}-R_{\min})} \times \exp[2i\pi(j-1)(i_0-1)/N] \times \tilde{\Psi}(k_j,t)\right]. \tag{30}$$

The outgoing flux imposes only positive values of j in Eq. (29); the negative components of F are numerically verified to be negligible [29]. $[F_{k_j}^+(t)]_{R_0}$ represents the part of the flux that leaves, at time t, the interaction region with a discretized velocity:

$$v_j = \frac{2\pi\hbar(j-1)}{M(R_{\max}-R_{\min})} . \tag{31}$$

With an initial wave packet normalized to unity,

$${}^{(c)}P_{k_j} = \int_{-\infty}^{+\infty}[{}^{(c)}F_{k_j}^+(t)]_{R_0}dt \tag{32}$$

gives the probability that the laser excitation leads to dissociation in channel (c), with fragments momentum k belonging to an interval $[k_j - \Delta k/2, k_j + \Delta k/2]$, where

$$\Delta k = \frac{2\pi}{(R_{\max}-R_{\min})} . \tag{33}$$

The total dissociation probability in channel (c) is simply given by

$${}^{(c)}P = \sum_{j=1}^{N/2}{}^{(c)}P_{k_j} , \tag{34a}$$

or equivalently by

$${}^{(c)}P = \int_{-\infty}^{+\infty}[{}^{(c)}F^+(t)]_{R_0}dt . \tag{34b}$$

III. APPLICATION TO H_2^+ MULTIPHOTON DISSOCIATION

The methodology so far developed is applied to the photodissociation of the $(v=0,j=1)$ rovibrational level of the H_2^+ ground state submitted to short electromagnetic pulses with strengths bridging intermediate- to strong-field limits. The ground and dissociative states that have been referred to correspond to $(1s\sigma_g)\,{}^1\Sigma_g^+$ and $(2p\sigma_u)\,{}^1\Sigma_u^+$, respectively. They are represented by Morse-type potentials. Their explicit form, and the R-dependent expression for the transition dipole moment $\mu_{gu}(R)$ with the values of corresponding parameters, are taken from Ref. [30]. The laser pulse of $\simeq$20-fs duration is given a symmetric Gaussian shape centered at $t_0 = 1000$ a.u. (25 fs),

$$\varepsilon(t) = \varepsilon_0 \exp\left[-\left[\frac{t-t_0}{\tau}\right]^2\right], \tag{35}$$

with $\tau = 333.3$ a.u. The maximum amplitude ε_0 is varied between 10^{-2} a.u. and 10^{-1} a.u., which roughly corresponds to a peak intensity varying from 3.5×10^{12} W/cm^2 (intermediate-coupling regime with the electronic Rabi frequency $\omega_R = \hbar^{-1}\mu\varepsilon_0$ of the same order of magnitude as the lowest vibrational frequency of H_2^+, $\omega_v \simeq 2000$ cm^{-1}) to 3.5×10^{14} W/cm^2 (strong-coupling regime, with $\omega_R \gg \omega_v$). The laser wavelength $\lambda = 329.7$ nm is chosen to introduce an energetically favorable vertical three-photon transition from the bound $(1s\sigma_g, v=0, j=1)$ to the continuum $(2p\sigma_u)$ state.

The maximum spatial extension retained for the wave packet is $[R_{\min}=0$ a.u., $R_{\max}=34$ a.u.], which is considered to be large enough when compared to the Morse potential well situated at $R=2$ a.u. and reaching its

asymptotic value for $R \simeq 8$ a.u. The number of quadrature points on this radial axis is taken to be $N=512$, such that the basis set on which the DVR Hamiltonian of Eq. (15) is displayed contains $2N=1024$ vectors. Moreover, this allows the scanning of fragment momenta (i.e., velocities) in the range $k \in [-47$ a.u., $+47$ a.u.] [Eq. (27)] corresponding to a maximum translational energy $E_{\max} \simeq 1.23$ a.u., which is approximately nine times the photon peak frequency ($E_{\max}=8.88\ \hbar\omega$). Multiphoton processes resulting into a final amount of three absorbed photons via virtual transitions involving five or six photons exchanged can thus be accurately described with such a basis.

For practical calculations, the outgoing flux is taken at $R_0=20$ a.u. [cf. Eq. (25)] and the outgoing wave packet is absorbed above $R=27$ a.u. using an exponential attenuation factor (which plays the role of an optical potential).

A. Results

The outcome of the calculation, before proceeding to any flux analysis, is the time-dependent behavior of the wave packet. This is illustrated in Figs. 2 and 3 for two different peak intensities taken as 1.4×10^{13} and 2.8×10^{14} W/cm^2 (representative of the intermediate and strong matter-field coupling regimes).

The upper parts display the square moduli of the wave-packet components ($\|\psi_u\|^2$ and $\|\psi_g\|^2$) in the continua of the excited $2p\sigma_u$ and the ground $1s\sigma_g$ states (the projections on the bound levels of the g state are not taken into consideration). The lower parts show on the same time scale the trajectories followed by the center-of-mass motion ($\langle R \rangle_g$ or $\langle R \rangle_u$) of the g or u components.

During the rise of the laser pulse (early excitation step: $t < 1000$ a.u.), similar overall behaviors, but with different amplitudes, are observed for the two intensities; i.e., an increase in $\|\psi_u\|^2$ driven by the pulse and following its time characteristics (shape and oscillations). Only a negligible amount of the wave packet is developed in the continuum of the ground state (i.e., $\|\psi_g\|^2 \ll \|\psi_u\|^2$).

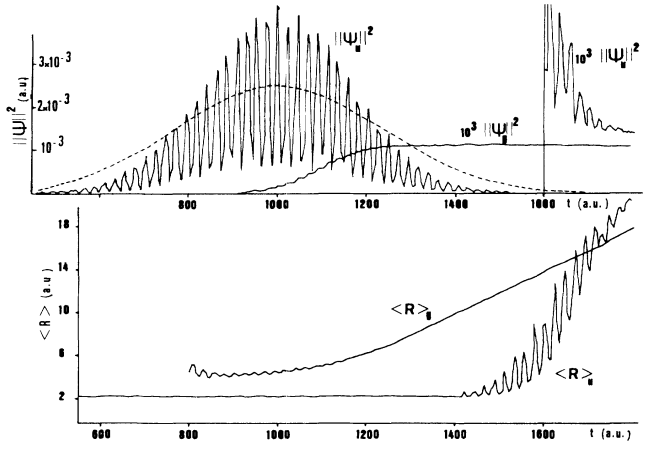

FIG. 2. Upper panel: square moduli of the wave-packet components $\|\psi_u\|^2$ and $10^3\|\psi_g\|^2$ in the continua of the u and g states as a function of time for a field intensity of $I=1.4\times10^{13}$ W/cm^2 (for $t > 1400$ a.u., $\|\psi_u\|^2$ is enlarged by a factor 10^3). The pulse shape is indicated, in arbitrary units, by the dotted line. Lower panel: center-of-mass mean value motion for the two components $\langle R \rangle_u$ and $\langle R \rangle_g$.

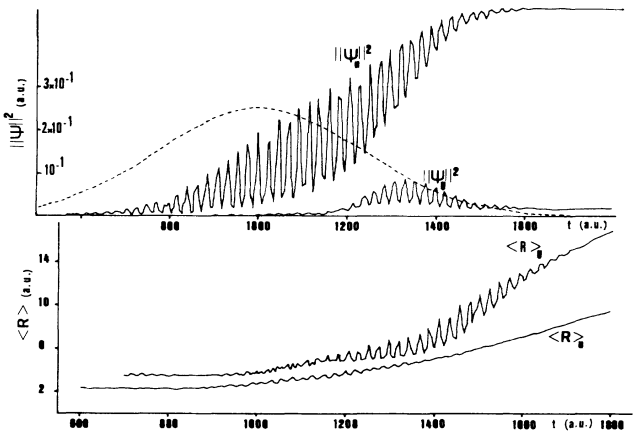

FIG. 3. Same as in Fig. 2 for a field intensity of $I=2.84\times10^{14}$ W/cm^2 (no enlargement is needed in the asymptotic region).

This initial phase of the excitation leads to quasi stationary wave packets: the center-of-mass mean values of the g and u components remain practically unchanged. More precisely, they correspond to $\langle R \rangle_u \simeq 2.20$ a.u. (Figs. 2 and 3) close to the equilibrium position of the field-free H_2^+ ion, and $\langle R \rangle_g \simeq 4$ and 3.6 a.u. (Figs. 2 and 3). This last value is roughly the abscissa of the crossing point between the dressed g and u channels, where the probability for a photon emission is enhanced (the energy gap 3.706 eV between g and u states at $R=3.6$ a.u. is close to the peak energy (frequency) 3.761 eV, of the laser).

Completely different behaviors are obtained during the falloff of the laser pulse for the two intensities. In the intermediate-coupling regime (Fig. 2), the excited-state component of the wave packet $\|\psi_u\|^2$ follows the driven electromagnetic field such that asymptotically (for $t=2000$ a.u., where $\langle R_u \rangle$ reaches 20 a.u.) only a very small fraction ($\simeq 10^{-3}$) of the early ($t=1000$ a.u.) wave packet ends up in channel u. The ground-state continuum component $\|\psi_g\|^2$ increases smoothly and reaches a comparable asymptotic value (at $t \simeq 1300$ a.u.). An inspection of the center-of-mass motions $\langle R \rangle_g$ or $\langle R \rangle_u$, shows that the u component starts to move towards the end of the pulse (at $t \simeq 1400$ a.u.), reflecting a post-pulse dissociating motion of the u-state population. A smooth trajectory is observed for the g component with a rather constant slope after $t=1200$ a.u.

In the strong-field regime (Fig. 3), the excited-state component keeps on rising even during the falloff of the laser pulse with decreasing amplitude oscillations to reach an asymptotic value 2.5 times larger than during the maximum of the pulse. It is also interesting to note that this value (related to the dissociation cross section) is 10^5 times the one that is obtained in the intermediate-field case. The continuum ground-state component shows an

oscillating behavior with a bell-shaped envelope with a maximum at $t \simeq 1350$ a.u. Its asymptotic value is approximately $\frac{1}{30}$ that of the u-state component. The $\langle R \rangle_u$ trajectory shows small-amplitude oscillations (around 2.2–3 a.u.) between $t=1000$ and $t=1350$ a.u., followed by a smooth and constant rise. The $\langle R \rangle_g$ trajectory has a similar behavior starting at $\simeq 4$ a.u., with a faster rise after $t=1350$ a.u.

The asymptotic-flow analysis can be performed in a time-resolved manner using a sudden perturbation technique. The laser pulse is suddenly cut at successive times t_i between 600 and 2000 a.u. and the post-pulse wave packet allowed to propagate in field-free conditions until the asymptotic region R_0 is reached. The results, in terms of relative dissociation probabilities as a function of t_i and the proton kinetic energy k_j,

$$ {}^{(c)}P_{k_j}(t_i) = \int_{-\infty}^{\infty} [{}^{(c)}F_{k_j}^{+}(t_i,t)]_{R_0} dt \ , \tag{36} $$

for the two field intensities under consideration are displayed in Figs. 4 and 5.

The vertical bars mark the resulting proton kinetic energy following the absorption of $n=1$, 2, or 3 photons of 3.761 eV. For very short times ($t<900$ a.u.), the early dynamics seems to proceed via a three-photon absorption in channel u in both intermediate- and strong-field cases. The main difference between the two intensity regimes is that the further time evolution leads to two comparable peaks corresponding to either two- or three-photon absorption and to dissociation in channels g or u, respectively, for $I=1.4\times10^{13}$ W/cm^2, whereas for $I=2.8\times10^{14}$ W/cm^2 but one peak is obtained describing one-photon absorption and dissociation in channel u. A closer inspection of the dynamical behavior (for $I=1.4\times10^{13}$ W/cm^2) shows how the dissociation probability in channel g corresponding to an overall two-photon absorption increases by taking non-negligible values from $t_i=1300$ a.u. and how the stabilization of the three-photon peak (channel u) occurs at $t_i=2000$ a.u. A different dynamical picture is observed in Fig. 5 (for $I=2.8\times10^{14}$ W/cm^2), where a progressive deformation of the relative dissociation probability on surface u leads from a three-photon to a one-photon absorption. A non-negligible dissociation probability on surface g with an overall two-photon absorption develops only temporarily during the falloff of the pulse.

The time-stabilized dissociation probabilities [cf. Eq. (32)] as a function of the proton kinetic energy (i.e., the so-called proton-energy spectra for different field intensities) are collected in Fig. 6. A closer inspection of the peaks reveals a Gaussian form (except for very-strong-field cases), whereas a Lorentzian behavior was obtained, in a previous calculation based on a cw laser, from which the common width for the resonance could be deduced

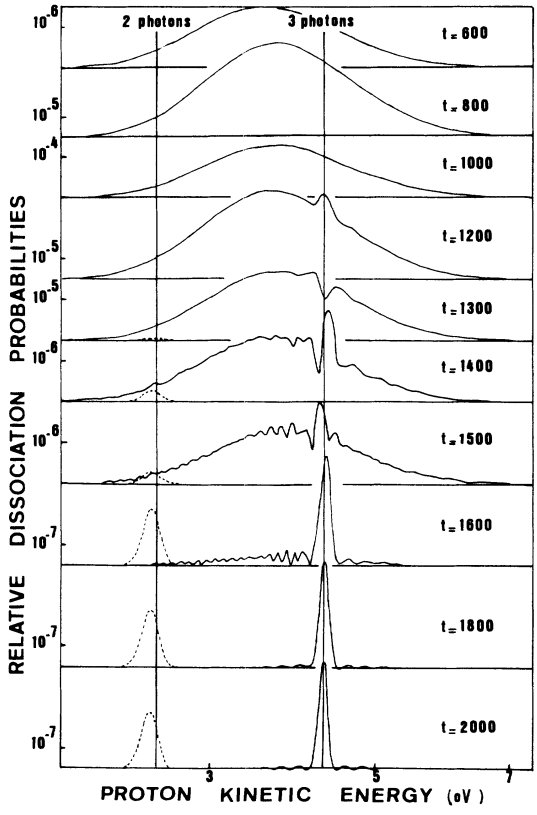

FIG. 4. Relative dissociation probabilities as a function of the proton kinetic energy (in eV) at different excitation times t(a.u.) for a field intensity of $I=1.4\times10^{13}$ W/cm^2. The solid and dotted lines correspond to a dissociation in the u and g states, respectively. The vertical lines represent the energies corresponding to two-, or three-photon absorptions.

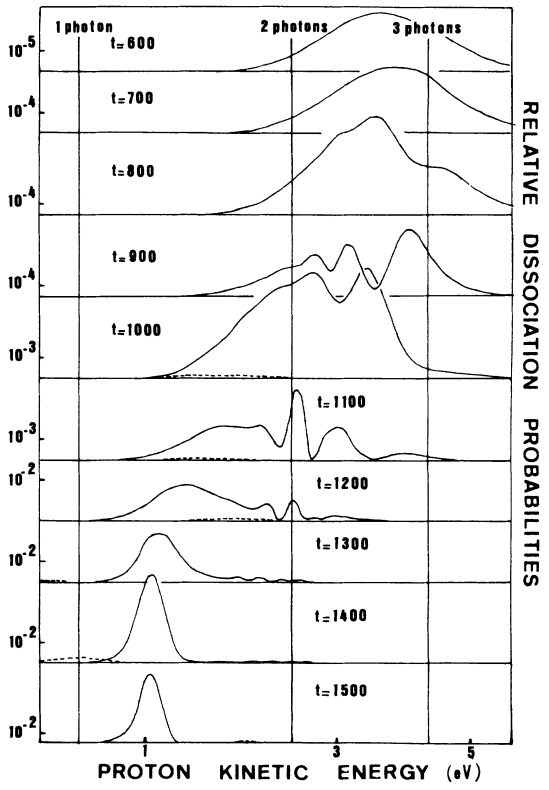

FIG. 5. Same as Fig. 4 for a field intensity of $I=2.84\times10^{14}$ W/cm^2.

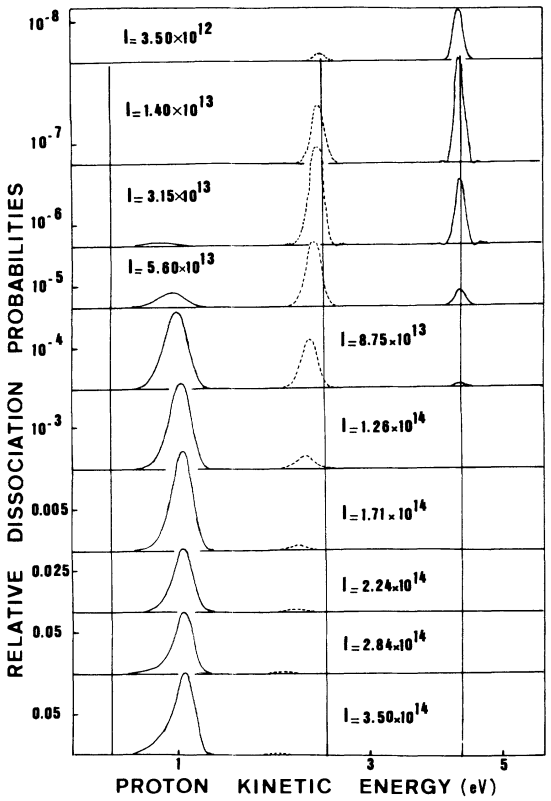

FIG. 6. Proton energy spectrum with varying intensities (in W/cm^2). The vertical lines represent the energies corresponding to one-, two-, or three-photon absorptions.

[5]. This is to be related with the pulsed character of the laser, which delivers several frequencies with different intensities. A spectra analysis, assuming absorption cross sections just equal to the intensity for a given frequency, leads to a modelization of the peaks with widths in fair agreement with that depicted in Fig. 5. (The full argument and derivation will be presented in a forthcoming paper [31].)

Apart from a considerable increase of dissociation probabilities with increasing field strengths, one observes a progressive shift of branching ratios from the three-photon peak that dominates at intermediate intensities (below 1.4×10^{13} W/cm^2) to the one-photon peak that prevails over the others at higher intensities (above 10^{14} W/cm^2). Intermediate situations, such that the one occurring for $I=5.6\times10^{13}$ W/cm^2, where the two-photon peak dominates, are also depicted. We note that the results are in qualitative agreement with the ones reported in Refs. [5,13].

Finally, the bulk of the information that can be reached concerns the total dissociation probabilities, regardless of the resulting proton kinetic energy. They are obtained either by calculating the area under each peak of Fig. 6 [as indicated by Eq. (34a)] or by direct time integration of the total outgoing flux [Eq. (34b)] [32]. Table I gathers the results for all laser intensities under consideration. The total dissociation probability is detailed into three parts that correspond to the three peaks of Fig. 6. Namely, ${}^{(c)}P_{(m\hbar\omega)}$ denotes the dissociation probability in channel c (i.e., g or u) resulting from an overall balance of m-photon absorption. It is important to note that, during the excitation step, more than m photons (say n) may be absorbed. Some of them are returned to the radiation field via stimulated emissions during the dissociation process itself. m represents the algebraic sum of absorbed ($+$) and emitted ($-$) photons. A qualitative way to reach n is to evaluate the intensity dependence I^n of the total dissociation probability. A local power law ($\propto I^n$) is indicated in Table I.

B. Discussion

The previous results offer sufficient information to elucidate the multiphoton exchange mechanisms taking place during dissociation in the intermediate- and strong-field coupling regimes. This discussion can conveniently be conducted by referring to the field-dressed diabatic and adiabatic channels of H_2^+ already considered in Ref. [5], which we reproduce in Fig. 7 for completeness.

1. *Intermediate field $I=1.4\times10^{13}$ W/cm^2*

According to Table I, the total dissociation probability obeys, in this regime, an intensity-dependence law in ap-

TABLE I. Dissociation probabilities in channel $c=(u$ or $g)$ resulting from $m=1$-, 2-, or 3-photon absorptions for varying field intensities. P_{total} is the total dissociation probability and n indicates the local intensity power law (I^n) that is followed.

I (W/cm^2)	${}^{(u)}P_{(\hbar\omega)}$	${}^{(g)}P_{(2\hbar\omega)}$	${}^{(u)}P_{(3\hbar\omega)}$	P_{total}	n
3.50×10^{12}	0.78×10^{-10}	0.5×10^{-8}	0.34×10^{-7}	0.39×10^{-7}	
1.40×10^{13}	0.64×10^{-8}	0.110×10^{-5}	0.145×10^{-5}	0.255×10^{-5}	3.02
3.15×10^{13}	0.876×10^{-6}	0.203×10^{-4}	0.851×10^{-5}	0.296×10^{-4}	3.02
5.60×10^{13}	0.561×10^{-4}	0.139×10^{-3}	0.210×10^{-4}	0.216×10^{-3}	3.45
8.75×10^{13}	0.135×10^{-2}	0.569×10^{-3}	0.325×10^{-4}	0.195×10^{-2}	4.93
1.26×10^{14}	0.142×10^{-1}	0.171×10^{-2}	0.365×10^{-4}	0.159×10^{-1}	5.75
1.71×10^{14}	0.755×10^{-1}	0.418×10^{-2}	0.326×10^{-4}	0.797×10^{-1}	5.23
2.24×10^{14}	0.235	0.888×10^{-2}	0.249×10^{-4}	0.243	4.18
2.84×10^{14}	0.478	0.170×10^{-1}	0.133×10^{-4}	0.495	3.03
3.50×10^{14}	0.709	0.307×10^{-1}	0.530×10^{-5}	0.739	1.89

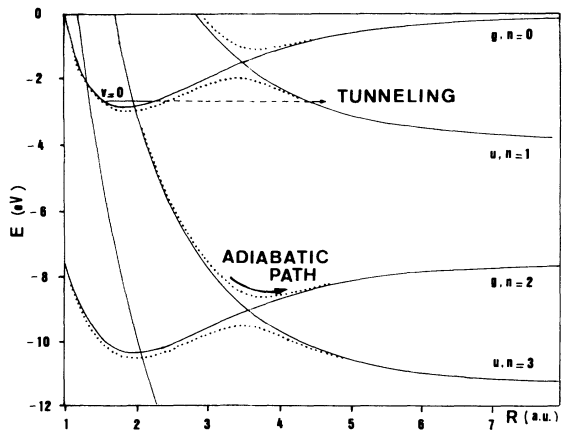

FIG. 7. Potential-energy curves of H_2^+ dressed with three photons of wavelength 329.7 nm. The solid lines correspond to the interacting diabatic channels. The dotted lines represent the field-dressed adiabatic curves after diagonalizing the radiative interaction for $I=1.4\times10^{13}$ W/cm^2 (taken from Ref. [5]).

proximately the third power I^3, indicating that the main mechanism is a three-photon absorption from channel $|g,n=0\rangle$ to channel $|u,n=3\rangle$. But, contrary to what occurs at lower intensities, the dissociation probability into channel $|g,n=2\rangle$ is no longer negligible, as can be seen from Fig. 6. The time evolution of the proton energy spectrum, displayed in Fig. 4, clearly indicates the way in which starting from a diffuse probability peak on an initial three-photon process changes the relative probabilities. The probability to dissociate into channel $|g,n=2\rangle$ takes on non-negligible values just after the pulse maximum ($t\simeq1200$ a.u.), and stabilized results are obtained for $t=2000$ a.u., with a total dissociation probability in channel $|u,n=3\rangle$ ($^uP_{3\hbar\omega}=0.145\times10^{-5}$), larger by a factor of 1.32 as compared to the one in channel $|g,n=2\rangle$ ($^gP_{2\hbar\omega}=0.110\times10^{-5}$). A comprehensive view of the dynamics is provided by Fig. 2. For the clarity of the discussion, we are considering three characteristic time domains: (i) $t\in[600$ a.u., 1000 a.u.], which corresponds to the early excitation step where the laser pulse is rising; (ii) $t\in[1000$ a.u.,1400 a.u.], which corresponds to the late excitation step where the laser pulse is falling off, and (iii) $t\in[1400$ a.u.,2000 a.u.], reflecting the asymptotic motion of the wave packet in approximate field-free conditions. During the rise of the pulse, the wave packet is prepared on the $|u,n=3\rangle$ channel driven by the laser field. Its corresponding component $\|\psi_u\|^2$ closely follows the oscillations and the shape of the pulse. Its center of mass is stationary around the equilibrium value of the ground state $\langle R\rangle_u\simeq2.2$. a.u. The population $\|\psi_g\|^2$ in the continuum of the $|g,n=2\rangle$ channel is negligible. Such a dynamical picture is consistent with a preparation step involving a vertical Franck-Condon (FC) jump from $|g,v=0,n=0\rangle$ induced by a three-photon absorption. After the pulse maximum, during the second half of the excitation, the population in channel $|u,n=3\rangle$, always driven by the field, decreases with it, and the center of mass of the corresponding wave packet $|\psi_u|^2$ is still stationary at $\langle R\rangle_u\simeq2.2$ a.u., which again is consistent with the FC vertical-jump model. Simultaneously, a small but non-negligible population smoothly rises in channel $|g,n=2\rangle$. Its center-of-mass mean value starts to increase at $\langle R\rangle_g\simeq4$ a.u., which roughly corresponds to the crossing distance of the dressed diabatic channels of Fig. 7. This is an indication that a small amount of the excited state ψ_u wave packet moves towards the crossing of $|u,n=3\rangle$ and $|g,n=2\rangle$ channels, where a photon emission takes place, bringing part of the population in channel $|g,n=2\rangle$. Such an interpretation has already been invoked in Ref. [5] when describing an implicit cw laser experiment [33]. At time $t=1400$ a.u., the laser pulse is almost over, and the remaining post-pulse populations in channels $|u,n=3\rangle$ and $|g,n=2\rangle$ move in approximately field-free conditions towards dissociation valleys. Concerning $\langle R\rangle_u$, there is an important acceleration with a subsequent mean velocity of $\simeq0.05$ a.u., whereas $\langle R\rangle_g$ shows a monotonic increase with a lower velocity of $\simeq0.02$ a.u. It is this slowing down of the protons by a stimulated emission during the process of fragmentation that has been referred to as a dissociative bremsstrahlung [5]. At $t=1600$ a.u., the proton energy spectrum is almost stabilized (Fig. 4), and the asymptotic-flow analysis done at $R=20$ a.u. (reached at $t\simeq2000$ a.u.) gives the relative total probabilities indicated in Table I. In summary, the leading mechanism is a three-photon FC vertical absorption from the ground state (intensity dependence law I^3), followed by stimulated photon emission occurring during the process of fragmentation (intensity dependence law I^4) and breaking the proton kinetic energy.

2. *Strong field $I=2.84\times10^{14}$ W/cm^2*

A more-complex situation occurs when very intense fields are considered. Figure 6 indicates a progressive change in the branching ratios, starting from a dominant three-photon peak at lower intensities, to a dominant two-photon peak at intermediate to strong intensities, to end up with a dominant one-photon peak for very strong fields. Such a one-photon peak seems unlikely at low intensities. At high intensities, however, two possible mechanisms can be involved; either (i) a five-photon process, $|g,n=0\rangle\rightarrow|u,n=3\rangle\rightarrow|g,n=2\rangle\rightarrow|u,n=1\rangle$, or (ii) a one-photon direct process $|g,n=0\rangle\rightarrow|u,n=1\rangle$, which can be competitive if the potential barrier of the adiabatic dressed curves (of Fig. 7) is lowered such that tunneling occurs as the leading process. This possibility has recently been suggested by Bandrauk [12] and discussed within a close-coupled calculation aiming to model a cw-laser experiment [13]. The intensity-dependence law of the total dissociation probability (Table I) indicates a change between I^5 and I when considering field strengths ranging from 2×10^{14} to 4×10^{14} W/cm^2, in fair agreement with the previous expectations. Figure 4 gives the time evolution of the proton energy spectrum, starting as in the intermediate-field case (the laser intensity at $t=600$ a.u. is very moderate) from a diffuse peak mainly centered on an initial three-photon absorption. The further evolution is very fast, and the one-photon peak is developed and stabilized very soon, after some large-

amplitude oscillations. A contribution to the two-photon peak from the ground-state continuum appears at $t=1000$ a.u. but remains very small.

The complete dynamical picture is displayed in Fig. 3. The early dynamics ($t<1000$ a.u., i.e., during the pulse rise) is roughly dominated by the same events as in the intermediate-field case. The initial, pulse-driven wave packet prepared on the excited $|u,n=3\rangle$ state by a vertical FC jump ($\langle R\rangle_u \simeq 2.2$ a.u. follows the oscillations of the field and remains stationary. The $\|\psi_g\|^2$ population is negligible.

A completely different scenario is valid during the second period of the excitation ($1000<t<1400$ a.u., i.e., during the pulse falloff), where the driven excited-state population $\|\psi_u\|^2$ increases considerably while its center of mass moves from $\langle R\rangle_u=2.2$. a.u. (at $t=1000$ a.u.) to $\langle R\rangle_u \simeq 4$ (at $t=1400$ a.u.). The ground-state continuum population $\|\psi_g\|^2$ increases in turn and presents a maximum value for $t\simeq 1350$ a.u. Its center-of-mass motion follows closely that of $\|\psi_u\|^2$. The two above-mentioned mechanisms are thus competing. At the pulse maximum, the adiabatic potential barrier between channels $|g,n=0\rangle$ and $|u,n=1\rangle$ is lowered enough to give access to the $|u,n=1\rangle$ channel by a direct one-photon absorption; this explains the important increase of $\|\psi_u\|^2$ after $t=1000$ a.u. and its mean localization at $\langle R\rangle_u=4$ a.u. (the position of the barrier). The part of the population of the excited state originating from the three-photon absorption proceeds adiabatically on channel $|g,n=2\rangle$ by stimulated emission of a photon at $\langle R\rangle_g \simeq 4$ (the position of the crossing point). This gives rise to an increasing and field-driven $\|\psi_g\|^2$. At $t\simeq 1350$ a.u., $\langle R\rangle_g$ and $\langle R\rangle_u$ have comparable values (4.5–5 a.u.), while a second photon is emitted from channel $|g,n=2\rangle$ to channel $|u,n=1\rangle$, resulting in a decrease of $\|\psi_g\|^2$ to the benefit of $\|\psi_u\|^2$. Later, field-free dynamics ($t>1400$ a.u.) yields the asymptotic motions of the wavepacket components. Again, contrary to the intermediate-coupling regime, there is a factor of 2 in the relative velocities of the ground- and excited-state components of the wave packet, but now it is the excited-state component that leads to less energetic protons, supporting the fact that the one-photon tunneling or the five-photon mechanism dominates over the three-photon $|g,n=0\rangle \rightarrow |u,n=3\rangle$ one. The final asymptotic flow analysis provides the figures displayed in Table I, indicating a total probability (${}^uP_{\hbar\omega}$) that is 28 times larger than (${}^gP_{2\hbar\omega}$), whereas (${}^uP_{3\hbar\omega}$) is negligible. In conclusion, the leading mechanism is a one-photon absorption (intensity dependence law) which is partly completed with a three-photon absorption, followed by the emission of two photons (intensity dependence law $\propto I^5$) during the fragmentation.

ACKNOWLEDGMENTS

One of the us (O.A.) wishes to thank Professor T. T. Nguyen Dang (Laval, Canada) for stimulating discussions. A grant of computing time from the Conseil Scientifique du Centre de Calcul Vectoriel pour la Recherche (C.C.V.R.) is gratefully acknowledged. This work is also supported by Cooperation France-Quebec ESR contract No. 010392.

[1] P. Agostini, F. Fabre, G. Mainfray, G. Petite, and N. Rahman, Phys. Rev. Lett. **42**, 1127 (1979); P. Kruit, J. Kimman, H. G. Muller, and M. J. Van der Wiel, Phys. Rev. A **28**, 248 (1983); R. M. Potvliege and R. Shakeshaft, *ibid.* **38**, 4597 (1988); M. Crance, J. Phys. B **21**, 2697 (1988).

[2] C. Cornaggia, D. Normand, J. Morellec, G. Mainfray, and C. Manus, Phys. Rev. A **34**, 207 (1986); J. W. J. Verschuur, L. D. Noordam, and H. B. Van Linden Van Den Heuvel, *ibid.* **40**, 4383 (1989).

[3] A. Zavriyev, P. H. Bucksbaum, H. G. Muller, and D. W. Schumacher, Phys. Rev. A **42**, 5500 (1990).

[4] P. H. Bucksbaum, A. Zavriyev, H. G. Muller, and D. W. Schumacher, Phys. Rev. Lett. **64**, 1883 (1990).

[5] A. Giusti-Suzor, X. He, O. Atabek, and F. H. Mies, Phys. Rev. Lett. **64**, 515 (1990).

[6] X. He, O. Atabek, and A. Giusti-Suzor, Phys. Rev. A **38**, 5586 (1988).

[7] R. Heather and H. Metiu, J. Chem. Phys. **88**, 5496 (1988).

[8] M. D. Feit, J. A. Fleck, Jr., and A. Steiger, J. Comput. Phys. **47**, 412 (1982).

[9] R. W. Heather, Comput. Phys. Commun. **63**, 446 (1991).

[10] R. W. Heather and F. H. Mies, Phys. Rev. A **44**, 7560 (1991).

[11] F. H. Mies and A. Giusti-Suzor, Phys. Rev. A **44**, 7547 (1991).

[12] A. D. Bandrauk, E. Constant, and J. M. Gauthier, J. Phys. II, France **1**, 1033 (1991).

[13] S. Miret-Artes, O. Atabek, and A. D. Bandrauk, Phys. Rev. A **45**, 8056 (1992).

[14] A. D. Bandrauk and M. L. Sink, J. Chem. Phys. **74**, 1100 (1981).

[15] A. Giusti-Suzor and F. H. Mies, Phys. Rev. Lett. (to be published).

[16] A. M. Lau and C. K. Rhodes, Phys. Rev. A **16**, 2392 (1978); J. M. Yuan and T. F. George, J. Chem. Phys. **68**, 3040 (1978); A. D. Bandrauk and T. T. Nguyen Dang, *ibid.* **83**, 2840 (1985).

[17] S. I. Chu, J. Chem. Phys. **75**, 2215 (1981).

[18] X. He, O. Atabek, and A. Giusti-Suzor, Phys. Rev. A **42**, 1585 (1990).

[19] A. D. Bandrauk and O. Atabek, in *Lasers, Molecules and Methods,* edited by J. O. Hirschfelder, R. E. Wyatt, and R. D. Coalson (Wiley, New York, 1989), Chap. XIX, p. 823.

[20] D. R. Bates, J. Chem. Phys. **19**, 1122 (1951).

[21] J. C. Light, I. P. Hamilton, and J. V. Lill, J. Chem. Phys. **82**, 1400 (1985).

[22] A. S. Dickinson and P. R. Certain, J. Chem. Phys. **49**, 4209 (1968).

[23] J. T. Muckerman, Chem. Phys. Lett. **173**, 200 (1990).

[24] G. Jolicard, J. Chem. Phys. **90**, 2320 (1989); G. Jolicard and J. Humbert, Comput. Phys. Commun. **63**, 216 (1991); G. Jolicard and G. D. Billing, Chem. Phys. **149**, 261 (1991).

[25] T. J. Park and J. C. Light, J. Chem. Phys. **85**, 5870 (1986).

[26] In our application, the dimension m of the subspace defined by the application of $H,(m-1)$ times to the initial vector is taken typically as 15 for a time step at $\Delta t=10$ a.u.

[27] R. C. Mowrey and D. J. Kouri, J. Chem. Phys. **84**, 6466 (1986); R. Heather and H. Metiu, *ibid.* **86**, 5009 (1987); **88**, 5496 (1988); D. Neuhauser, M. Baer, R. S. Judson, and D. J. Kouri, Chem. Phys. Lett. **169**, 372 (1990).

[28] R. N. Dixon, C. C. Marston, and G. G. Balint-Kurti, J. Chem. Phys. **93**, 6520 (1990).

[29] This check has actually been worked out within an accuracy of $\simeq 10^{-4}$.

[30] F. V. Bunkin and I. I. Tugov, Phys. Rev. A **8**, 601 (1973).

[31] G. Jolicard and O. Atabek (unpublished).

[32] The two methods lead to results in agreement within 3–4 figures of accuracy (relative error better than 10^{-3}).

[33] We note that the agreement with the result of Ref. [5] is only quantitative due to the difference in pulse shape for the lasers in consideration: the only characteristic they share is their peak intensity and frequency.